with ferricline deepening (Radenac et al. 2001; Wang et al. 2005) and with a negative anomaly of chlorophyll (see Figure 1.5.3 in Section 1.5). The time series of the nitrate anomaly (signal previously detrended and deseasonalised) over 40°S–40°N region (Figure 1.6.3) shows a strong correlation between nitrate concentration and ENSO index.

At the regional scale, other processes can play important roles in shaping nutrient distribution. As an interesting example, the Mediterranean Sea (Figure 1.6.4(a), product reference 1.6.2) shows a spatial pattern of nutrient distribution that depends on the superposition of inverse estuarine circulation of the Atlantic water inflowing from the Gibraltar Straits, local areas of upwelling (i.e. north-western Mediterranean Sea and Southern Adriatic Sea), an uneven distribution of rivers, and – most importantly – the activity of plankton autotrophs, which depletes nutrient concentration along the Atlantic modified water while enriching through their sinking the outflowing deeper waters (i.e. the clearly shown east to west gradient in the subsurface 0–150 m map, Figure 1.6.4(b)). In 2016, the anomaly map (Figure 1.6.4(c)) highlights a generally lower than average value of nitrate concentration, more evident in specific areas (e.g. north-western Mediterranean, south-eastern Tyrrhenian Sea, north-western Ionian Sea, south-eastern Aegean Sea, central Levantine), which is related to a general negative anomaly of the mixed layer depth (not shown), and therefore to a stronger water column stratification. The positive anomaly observed along the Italian coast of the Adriatic Sea is related to the 2016 phytoplankton negative anomaly, as prescribed by the assimilated ocean colour chlorophyll (Figure 1.5.3) and the climatological (i.e. constant in years) nutrient river discharge rates.

1.7. Air-to-sea carbon flux

Leading authors: Coralie Perruche, Cosimo Solidoro

Contributing authors: Gianpiero Cossarini

Statement of outcome: In this new section of the Ocean State Report, we study the sea-to-air CO_2 flux as described by a global and a regional coupled physical-biogeochemical model. At the global scale, the model simulates a relatively stable ocean carbon uptake during the 1990s and a sharp increase since the beginning of the 2000s. In the Mediterranean Sea, model results indicate that it acts as a weak sink during the last decade. In 2016, there is a strong negative anomaly of the equatorial Pacific outgassing due to a weaker upwelling (end of El Niño event).

Products used:

Ref. no.	Product name and type	Documentation
1.7.1	GLOBAL_REANALYSIS_BIO_001_018 Reanalysis	PUM: http://marine.copernicus.eu/documents/PUM/CMEMS-GLO-PUM-001-018.pdf QUID: http://marine.copernicus.eu/documents/QUID/CMEMS-GLO-QUID-001-018.pdf
1.7.2	MEDSEA_REANALYSIS_BIO_006_018 Reanalysis	PUM: http://marine.copernicus.eu/documents/PUM/CMEMS-MED-PUM-006-008.pdf QUID: http://marine.copernicus.eu/documents/QUID/CMEMS-MED-QUID-006-008.pdf

The concentration of atmospheric CO_2 has exceeded 400 ppm in 2015 and has thus increased by about 40% from about 280ppm in the pre-industrial era (Conway et al. 1994, Masarie and Tans 1995, www.esrl.noaa.gov/gmd/ccgg/trends/). This increase would have been much stronger without the contribution of the ocean and land biospheres which absorb each year roughly one half (25% ocean and 25% land) of the anthropogenic carbon emissions (Le Quéré et al. 2016, Ballantyne et al. 2012). The CO_2 flux is directly linked to the CO_2 partial pressure (pCO_2) in the ocean (product no. 1.7.1, 1.7.2) and in the atmosphere, but also to CO_2 solubility in sea water and to wind speed (Sarmiento and Gruber 2006, Takahashi et al. 2002, Wanninkhof 1992).

A few processes called 'pumps' are driving the air–sea exchange of CO_2 and the vertical distribution of carbon in the ocean. The ocean CO_2 partial pressure is prominently controlled by the physico-chemical pump of solubility which increases as temperature and salinity fall. CO_2-enriched water masses are then trapped below the thermocline where deep water convection occurs. As a consequence, the solubility pump is stronger at high latitudes. The second pump is the so-called 'organic carbon pump', which refers to biological processes that sustain a vertical downward flux of carbon (Sarmiento and Gruber 2006, Gehlen et al. 2011). Through photosynthesis, phytoplankton absorbs dissolved inorganic carbon (DIC) in the surface sunlight layer (euphotic zone) to build organic matter, which is then remineralised in the ocean interior into DIC after particle sinking. The third pump – the 'carbonate pump' – has a negative feedback on ocean carbon uptake as it counteracts the downward flux of DIC into the deep ocean (Gehlen et al. 2011). This process involves calcifiers – plankton species such as coccolithophores (phytoplankton) or foraminifera (zooplankton). To build their carbonate shell, they absorb DIC and release CO_2.

The superposition of those pumps results in large regional variability in the distribution of the sea-to-air flux of CO_2. Figure 1.7.1 is a climatological mean of these CO_2 fluxes computed from the CMEMS global biogeochemical reanalysis product (product reference 1.7.1). The ocean acts as a carbon sink at high latitudes (40–60° in both hemispheres) due to the combined effect of cooling/formation of deep water in winter and of biological activity (strong seasonal bloom in this area) in spring (Takahashi 2002). High wind speeds over these low pCO_2 waters increase the ocean uptake (Takahashi 2002). In upwelling systems (equatorial upwelling, eastern boundary upwelling system, Arabian Sea upwelling), the ocean is a source of CO_2 for the atmosphere due to the upwelling of CO_2-rich waters (Figure 1.7.1). In the Pacific Ocean, the upwelled water masses at the equator are then advected westward and poleward due to equatorial divergence within the subtropical cells (Schott et al. 2004). Besides this climatological view, there is a strong interannual variability, in particular in regions with strong climate modes (Resplandy et al. 2015), i.e. Pacific Decadal Oscillation, North Atlantic Oscillation, Southern Annual Mode in high latitudes and El Niño Southern Oscillation in tropical Pacific. In 2016, a significant negative CO_2 flux anomaly in the tropical Pacific (Figure 1.7.2) highlights the signature of El Niño during the beginning of the year (see Figure 2.6.1 of Section 2.6: this CO_2 flux anomaly is associated with a positive anomaly of surface temperature). The less intense upwelling leads to reduced outgassing in the tropical Pacific.

Atmospheric measurements and CO_2 emission inventories show a global increase of ocean and land carbon uptake over the past 50 years (Ballantyne et al. 2012, Le Quéré et al. 2017). In the framework of the Global Carbon Project (http://www.globalcarbonproject.org/about/index.htm), an annual assessment of the global budget is done each year (Le Quéré et al. 2017). During the last decade (2007–2016), anthropogenic air-to-sea carbon flux amounts to 2.4 ± 0.5 PgC/year (Le Quéré et al. 2017). In 2016, the ocean sink was 2.6 ± 0.5 PgC/year (Le Quéré et al. 2017). These global budget estimations (Le Quéré et al. 2017) are based on observations from the 1990s (mean) and on Earth System Models (annual anomalies and trends). Figure 1.7.3 presents the model estimation of the net integrated sea-to-air carbon flux compared with estimates of Landschützer et al. (2014) and Rödenbeck et al. (2015) based on data-driven mapping methods applied on SOCAT database (surface ocean pCO_2 measurements: http://www.socat.info/, Bakker et al. 2014). It shows a good comparison between these products with a relatively stable ocean carbon uptake during the 1990s and a sharp increase since the beginning of the 2000s. This may be related to a weakening of the upper-ocean overturning circulation (DeVries et al. 2017), but needs further investigations. In 2016, our model simulates a global ocean uptake of 2.2 PgC/year. To obtain the global anthropogenic atmosphere-ocean CO_2 flux, we have to add the natural river outgassing of 0.45 PgC/year (Jacobson et al. 2007). It gives an anthropogenic CO_2 flux of 2.65 PgC/year that is in line with Le Quéré et al.'s (2017) estimation.

The different estimations of the global air–sea carbon flux agree on the current buffer capacity of the ocean to alleviate the greenhouse effect and the associated climate warming. A lot of uncertainties still remain in the different estimates of the global flux due to the scarcity of data and the coarse resolution/complexity of

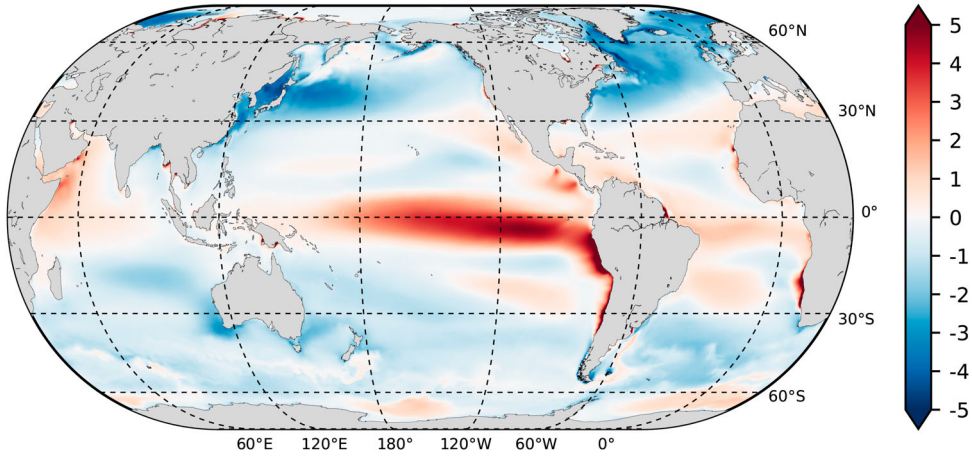

Figure 1.7.1. Net sea-to-air flux for CO_2 (mol. C/m^2/year) computed from the CMEMS global reanalysis (product reference 1.7.1) over the period 1993–2014. Positive values represent a flux from the ocean to the atmosphere (outgassing).

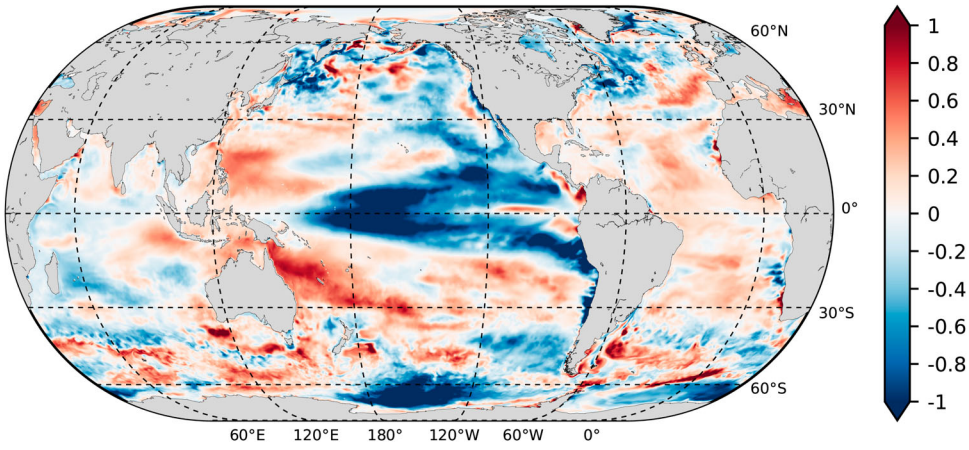

Figure 1.7.2. Anomalies of net sea-to-air flux of CO_2 (mol. C/m^2/year) in 2016 relative to climatological period 1993–2014. At each grid cell, the time series was previously detrended. Our simulation starting from WOA and GLODAP climatologies and being relatively short, we prefer removing the trend to filter the model drift.

physical and biogeochemical processes in models. But Earth System Models (Roy et al. 2011; Ciais et al. 2013 (IPPC WG1, chapter 6); Séférian et al. 2014) ultimately predict a decrease of ocean carbon uptake due to the warming of surface layers (decrease of CO_2 solubility) (Roy et al. 2011), enhanced ocean stratification (less ventilation and carbon export by mixing) (Séférian et al. 2012) and biogeochemical processes (ocean acidification, deoxygenation, reduced primary productivity) (Bopp et al. 2013) in the next century. However, the ocean response to the climate change is still a matter of debate.

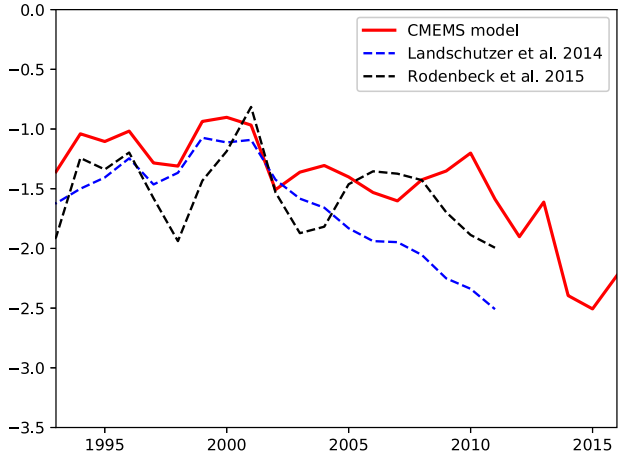

Figure 1.7.3. Annual time series of net sea-to-air flux of CO_2 (PgC/year). (Blue) Landschützer et al. (2014) product: a neural network is used to reconstruct the non-linear relationship between external drivers (SST, SSS, MLD, Chla and atmospheric pCO_2) and SOCATv2 pCO_2 database. Downloaded on the SOCOM (Surface Ocean pCO_2 Mapping intercomparison) website: http://www.bgc-jena.mpg.de/SOCOM/ (black) Rödenbeck et al. (2015) product: statistical interpolation scheme with SOCATv3 pCO_2 database. RED, the CMEMS global reanalysis (product reference 1.7.1).

By offering products that result from the combination of state-of-the-art observations and higher resolution models specifically designed to describe the characteristics of a given system, CMEMS regional systems can provide more accurate analyses and forecasts of a regional area making them ideally placed to inform this debate going forward. Figure 1.7.4 illustrates the spatial distribution of the mean climatological annual pCO_2 (ppm) and net air–sea fluxes for CO_2 (gC/m^2/y) over the period 1999–2014 in the Mediterranean Sea (product reference 1.7.2).

Results of the Mediterranean regional reanalysis provide a more detailed description of the spatial variability in the regional sea, especially along the shelves, which are known to be important when computing carbon budgets at the global scale (Bauer et al. 2013, Bourgeois et al. 2016). Reanalysis results indicate that in the last decade, the Mediterranean Sea, as a whole, acted as a weak sink of atmospheric carbon (around −3.5 TgC/year in average over the 1999–2014 period). Furthermore, we observe that while the climatology derived from the Mediterranean model returns a more detailed picture of the spatial distribution of CO_2 fluxes over the Mediterranean Sea in respect of the one provided by the global model, both climatologies agree in indicating that there was an outgassing on the southern parts of the Mediterranean Basin and an ocean uptake in its northern parts. In this context it is worth noting that biological activity plays a significant role in carbon sequestration ecosystem services in the Mediterranean Sea: as an example, Melaku Canu et al. (2015) showed that without it the Mediterranean would be a globally significant source of CO_2, and quantified the

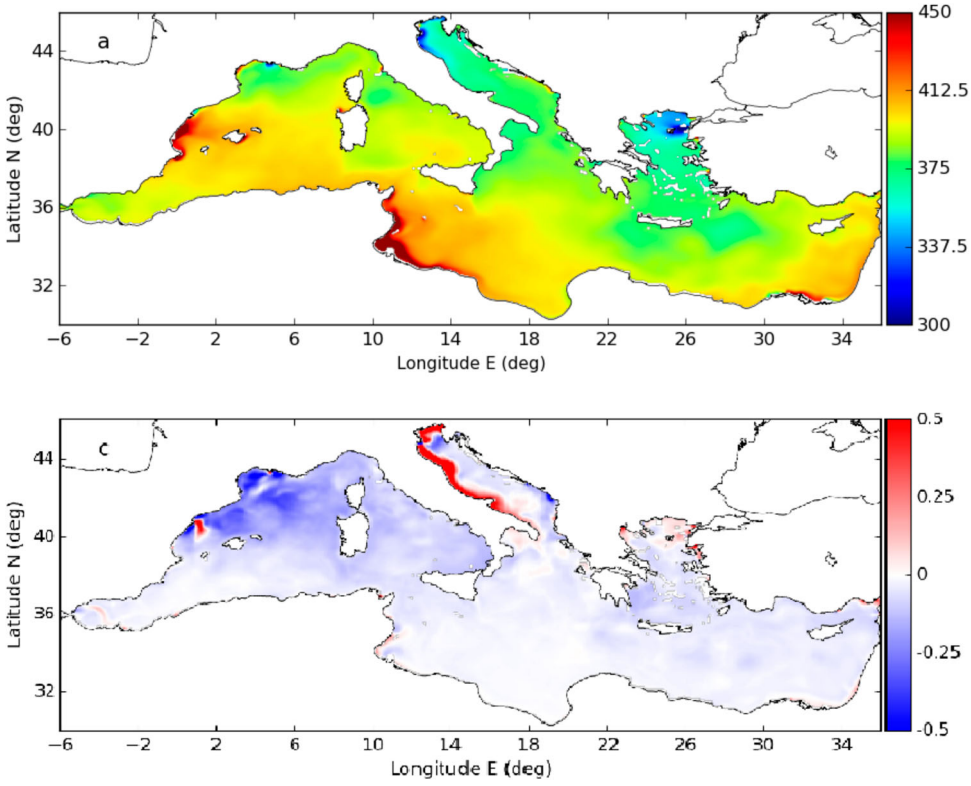

Figure 1.7.4. Climatological mean (1999–2014) of ocean pCO_2 (a, ppm) and net sea-to-air flux for CO_2 (b, mol. C/m^2/year, positive values represent a flux from the ocean to the atmosphere, i.e. outgassing) derived from product reference 1.7.2.

contribution of plankton carbon sequesteration value between €100 and €1500 million annually for the Mediterranean Sea.

Since direct experimental observations of pCO_2 are too scarce and do not cover the basin scale, it is not possible to have a direct assessment of the errors on this parameter. However, it is possible to derive an indirect estimate of the uncertainty on pCO_2 by combining the uncertainties on alkalinity and on DIC, and using the error propagation equation. This produces a conservative estimate of pCO_2 uncertainty in the surface layer of about 50ppm. The uncertainties on alkalinity and DIC were produced by comparing observation-based climatologies to model-based climatologies (QUID of product reference 1.7.2).

The pCO_2, and the related CO_2 atmospheric fluxes, shows a strong seasonal cycle (Figure 1.7.5) as linked to temperature changes and trophic dynamics. Superposed are interannual changes (Figure 1.7.5) which may be related to interannual variability in physical or biogeochemical parameters, but also to changes in the input and exchanges with the system boundaries, i.e. linked to properties of Atlantic water inflowing from Gibraltar straits (Cossarini et al. 2015).

Figure 1.7.5(b) highlights both the seasonal and interannual variability, and shows that over the last 15 years there is a slightly negative multiannual trend in the basin means of the sea-to-air CO_2 flux which is the response to the increase of atmospheric pCO_2 from 360 to 399 (data of Lampedusa station from World Data Centre for Greenhouse gases 2017). Spatial distributions also vary from year to year, in response to changes in biological productivity, surface temperature and transport processes. Anomalous changes during the year 2016 (rel. to the 1999–2014 reference period) indicate that in the last year the fluxes from the atmosphere to the ocean are slightly higher (Figure 1.7.5(a)) compared to the climatological mean (i.e. the mean annual value of 2016 equals to -3.5 gC/m^2/year). As it can be seen from the anomaly map (Figure 1.7.5), differences are not homogenously distributed in space, but depend on, and track effects of, general circulation and even mesoscale features. In particular, one can observe Atlantic water spreading into the western part of the Mediterranean and along the African coast, as well as relevant changes in the Levantine basin, which are possibly related to the temperature regime, and

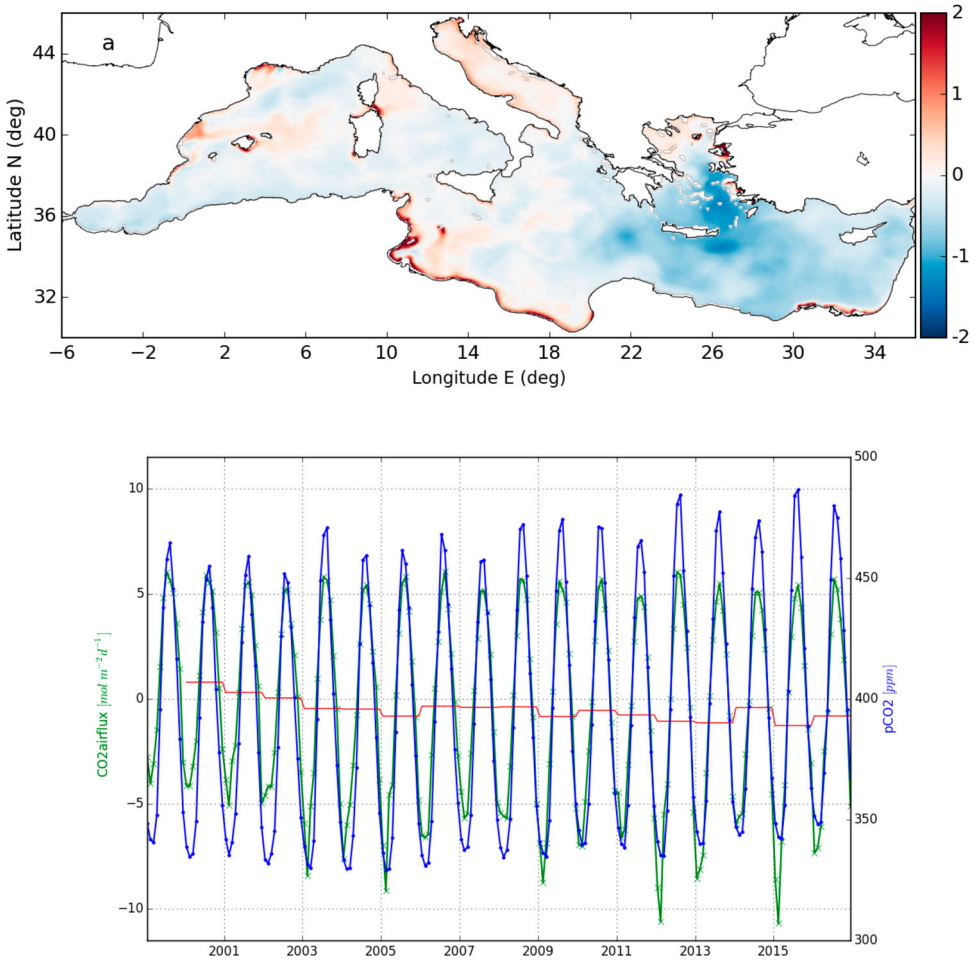

Figure 1.7.5. (a) Anomalies during 2016 (relative to the climatology reference shown in Fig. 1.7.4) of net sea-to-air CO_2 flux (mol. C/m^2/year) derived from the product reference 1.7.2. (b) Monthly (green line) and annual mean (red line) sea-to-air CO_2 fluxes (mmolC/m^2/d, first axis, positive values represent a flux from the ocean to the atmosphere, i.e. outgassing) and monthly ocean partial pressure of CO_2 (pCO_2, [ppm], blue line, second axis) for the years 1999–2016. Values refer to spatial averages over the entire Mediterranean Sea basin, and are derived from product no. 1.7.2.

positive anomalies in the Adriatic Sea and along the coasts of the Ionian and Levantine seas.

1.8. Wind

Leading author: Ad Stoffelen

Contributing authors: Jos de Kloe, Ana Trindade, Daphne van Zanten, Anton Verhoef, Abderahim Bentamy

Statement of outcome: Global and regional decadal trends in marine wind and stress forcing are now available through stable satellite instrument records, providing more detailed evidence of the changing climate. In 2016, a prominent anomaly stands out in the Arctic region over the Atlantic with poleward winds, specifically for the months of September, October and November.

Products used:

Ref. No.	Product name & type	Documentation
1.8.1	WIND_GLO_WIND_L3_NRT_OBSERVATIONS_012_002 Remote sensing	PUM: http://marine.copernicus.eu/documents/PUM/CMEMS-OSI-PUM-012-002.pdf QUID: http://marine.copernicus.eu/documents/QUID/CMEMS-OSI-QUID-012-002-003-005.pdf
1.8.2	WIND_GLO_WIND_L3_REP_OBSERVATIONS_012_005 Remote sensing	PUM: http://marine.copernicus.eu/documents/PUM/CMEMS-OSI-PUM-012-002.pdf, QUID: http://marine.copernicus.eu/documents/QUID/CMEMS-OSI-QUID-012-002-003-005.pdf
1.8.3	WIND_GLO_WIND_L4_NRT_OBSERVATIONS_012_004 Remote sensing	PUM: http://marine.copernicus.eu/documents/PUM/CMEMS-OSI-PUM-012-004.pdf QUID: http://marine.copernicus.eu/documents/QUID/CMEMS-OSI-QUID-012-002-003-005.pdf

(*Continued*)